REPORT DOCUMENTATION PAGE

Form Approved
OMB No. 0704-0188

1. REPORT DATE *(DD-MM-YYYY)*	**2. REPORT TYPE**	**3. DATES COVERED** *(From - To)*
July 2015	Technical Paper	July 2015-July 2015

4. TITLE AND SUBTITLE
Exploration of POD-Galerkin Techniques for Developing Reduced Order Models of the Euler Equations

5a. CONTRACT NUMBER

5b. GRANT NUMBER

5c. PROGRAM ELEMENT NUMBER

6. AUTHOR(S)
Mundis, N., Edoh, A. and Sankaran, V.

5d. PROJECT NUMBER

5e. TASK NUMBER

5f. WORK UNIT NUMBER
Q12J

7. PERFORMING ORGANIZATION NAME(S) AND ADDRESS(ES)

Air Force Research Laboratory (AFMC)
AFRL/RQR
5 Pollux Drive
Edwards AFB, CA 93524-7048

8. PERFORMING ORGANIZATION REPORT NO.

9. SPONSORING / MONITORING AGENCY NAME(S) AND ADDRESS(ES)
Air Force Research Laboratory (AFMC)
AFRL/RQR
5 Pollux Drive
Edwards AFB CA 93524-7048

10. SPONSOR/MONITOR'S ACRONYM(S)

11. SPONSOR/MONITOR'S REPORT NUMBER(S)
AFRL-RQ-ED-TP-2015-284

12. DISTRIBUTION / AVAILABILITY STATEMENT
Distribution A: Approved for Public Release; Distribution Unlimited.

13. SUPPLEMENTARY NOTES
Technical Paper and Presentation presented at AIAA Propulsion and Energy Conference; Orlando, FL; 2015 July 27-29. PA#15401.

14. ABSTRACT
Investigations of relevant issues involved in developing a reduced order model (ROM) are performed for describing combustion response to specific excitations using Euler equations as a continued work from a previous studies using a reaction-advection scalar equation. The ROM is obtained by employing Galerkin's method to reduce the high-order PDEs to a lower-order ODE system by means of POD eigen-bases. For purposes of this study, a linearized version of the Euler equations is employed. The knowledge obtained from previous scalar equation studies is applied to ROM development of Euler equations. Numerical stability issues are encountered in Euler equation studies, the cause of which is narrowed down to normalization methods for vector variables. The effects of normalization methods are then further assessed in terms of the ROM characteristics and its predictive capability.

15. SUBJECT TERMS

16. SECURITY CLASSIFICATION OF:			**17. LIMITATION OF ABSTRACT**	**18. NUMBER OF PAGES**	**19a. NAME OF RESPONSIBLE PERSON**
					Venke Sankaran
a. REPORT	**b. ABSTRACT**	**c. THIS PAGE**	SAR	20	**19b. TELEPHONE NO** *(include area code)*
Unclassified	**Unclassified**	**Unclassified**			661-275-5534

Exploration of POD-Galerkin Techniques for Developing Reduced Order Models of the Euler Equations

Cheng Huang[*], William E. Anderson[†], Charles L. Merkle[‡]

Purdue University, West Lafayette, IN, 47907

and

Venkateswaran Sankaran[§]

Air Force Research Laboratory (AFRL), Edwards AFB, CA, 93524

Investigations of relevant issues involved in developing a reduced order model (ROM) are performed for describing combustion response to specific excitations using Euler equations as a continued work from a previous studies using a reaction-advection scalar equation. The ROM is obtained by employing Galerkin's method to reduce the high-order PDEs to a lower-order ODE system by means of POD eigen-bases. For purposes of this study, a linearized version of the Euler equations is employed. The knowledge obtained from previous scalar equation studies is applied to ROM development of Euler equations. Numerical stability issues are encountered in Euler equation studies, the cause of which is narrowed down to normalization methods for vector variables. The effects of normalization methods are then further assessed in terms of the ROM characteristics and its predictive capability.

I. Introduction

Combustion instability is a complex phenomenon that results from the coupling between the modes of heat release and acoustics. In practical combustor devices the complexity is greatly amplified by turbulent, compressible flow, very high rates of heat release, and often complicated geometries and acoustic boundary conditions. Modern computational capability offers the potential for moving beyond the empirically-based design analysis of the past, but simulations of full scale dynamics for engineering analysis are still out of reach. However, high fidelity

[*] Graduate Research Assistant, School of Mechanical Engineering and Student Member AIAA.
[†] Professor, School of Aeronautics and Astronautics and Associate Fellow AIAA.
[‡] Professor Emeritus, AIAA Member.
[§] Senior Scientist, Rocket Propulsion Division and Senior Member AIAA.

simulations of smaller scale domains can be used to obtain reduced order models of the combustion response that can presumably provide accurate descriptions of the linear/nonlinear coupling between acoustics and combustion.

The model reduction techniques have been well studied to develop numerically stable and robust reduced order models (ROM) [1-3]. ROM techniques have wide application in non-reacting flow problems including flow control [4-6] and unsteady aeroelasticity [7, 8]. Recently application has been extended to combustion problems [9, 10]. A preliminary exploration of the POD/Galerkin technique using a model reaction-advection scalar equation in developing valid and capable reduced-order model was performed by Huang et al. [11], which mainly assesses the capability of the ROM for predicting responses at target frequencies. Other than the implementation of techniques in practical problems, focuses have also been placed on resolving the robustness and stability issues in developing a valid reduced order model. As reported, the issues can come from the possible inherent lack of numerical stability in the POD/Galerkin method itself [12], truncation of low-energy dissipative POD modes [1] and simplifications of higher-order equations [13]. The balanced POD technique has been proposed to build numerically stable ROM for linear systems [2, 14]. Bergmann et al. proposed to add residuals of the Navier-Stokes equations to account for the absence of low-energy dissipative POD modes [1]. Barone et al [15, 16] proposed to stabilize the reduced system by symmetrizing the higher-order PDE with a preconditioning matrix. Rowley et al. also pointed out that defining a proper inner product can be important when dealing with model reduction of the Navier-Stokes equations [3].

In this paper, we extend our previous exploratory work using a representative scalar equation [11] to vector equations. The remainder of the paper is organized as follows. In Section II, a summary of previous work and major conclusions is given. In Section III, we present the Euler equations with a modeled combustion source term used in the present study as well as the Galerkin formulation and POD techniques for deriving reduced order models for the linearized version of the equation. In Section IV, we describe the test problem and the representative characteristics of the CFD solutions used in the ROM studies. In Section V, we follow the procedures developed in our previous scalar equation studies. First, we validate the resulting POD eigen-bases and ROMs. Second a specific numerical stability issue is identified during ROM development that can be attributed to the normalization methods used in generating the POD eigen-bases for vector variables. Based on that, the effects of normalization methods on ROM development are further evaluated. In the final section, we provide some concluding remarks and future directions for continued research and development.

II. Review of Scalar Equation Studies

A review of previous work using a reaction-advection scalar equation [11] is given in this section. A Galerkin approach based upon Proper Orthogonal Decomposition (POD) techniques is used to assess the performance and capabilities of the derived reduced solver. The model equation is posed in a non-linear form but linearized versions are used also to allow more detailed investigation of the impact of source term,

$$\text{Model Equation:}\quad \frac{\partial\theta(X,\tau)}{\partial\tau}+\frac{\partial\theta(X,\tau)}{\partial X}=K_1\left[1-\theta(X,\tau)\right]\theta(X,\tau)+K_1\theta_T\left[\theta(X,\tau)-\bar{\theta}(X)\right]$$
$$\text{Linearized Version:}\quad \frac{\partial\theta'(X,\tau)}{\partial\tau}+\frac{\partial\theta'(X,\tau)}{\partial X}=K_1\left[1+\theta_T-\bar{\theta}(X)\right]\theta'(X,\tau) \tag{1}$$

The approach uses numerical solutions of the model equation, obtained by perturbing quantities of interest such as the inlet conditions, as the database for building a set of POD eigen-bases. The POD-derived eigen-bases are, in turn, used to obtain an ordinary differential equation, which constitutes the ROM. Once the ROM is established, it can be used as lower-order test-bed to predict detailed results within certain parametric ranges at a fraction of the cost of the full governing equations. Major conclusions from the studies using the linearized model scalar equation are summarized below and further applied in the Euler equations studies given in the next section:

1. In POD eigen-bases generation, for cases where the numerical rank of POD matrix is equal to the analytical rank, the number of POD modes is twice the number of frequencies included in the forcing function;
2. Consistent discretization between the CFD solution and the ROM is required to obtain good accuracy;
3. Including the same number of POD modes as the rank of POD matrix is needed to reproduce the original CFD solution;
4. The eigenvalue spectrum of the ROM stiffness matrix can be helpful in identifying possible numerically unstable modes;
5. The ROM obtained from single-frequency forcing is able to provide reasonable predictions at only the forcing frequency; applying forcing functions with richer frequency content provides significant enhancement in the predictive capability of the resulting ROM's.

III. Formulation

A. Governing equations

The governing equations are the quasi-one-dimensional unsteady Euler equations with a single-step chemical reaction and a specified reaction distribution:

$$\frac{\partial\mathbf{Q}}{\partial t}+\frac{\partial\mathbf{E}}{\partial x}=\mathbf{H}+\mathbf{H}_f+\mathbf{H}_q \tag{2}$$

where,

$$\mathbf{Q}=\begin{pmatrix}\rho A\\ \rho uA\\ eA\\ \rho Y_{ox}A\end{pmatrix},\ \mathbf{E}=\begin{pmatrix}\rho uA\\ \left(\rho u^2+p\right)A\\ \left(e+p\right)A\\ \rho uY_{ox}A\end{pmatrix},\ \mathbf{H}=\begin{pmatrix}0\\ p\dfrac{dA}{dx}\\ 0\\ 0\end{pmatrix},\ \mathbf{H}_f=\begin{pmatrix}\dot{\omega}_f\\ \dot{\omega}_f\bar{u}\\ \dot{\omega}_f\left(\bar{h}_0-\dfrac{\bar{p}}{\bar{\rho}}\right)\\ -\dot{\omega}_{ox}\end{pmatrix},\ \mathbf{H}_q=\begin{pmatrix}0\\ 0\\ \dot{q}'''\\ 0\end{pmatrix}.$$

Here x and t are the space and time variables, ρ is the density, u is the velocity, e is the total energy, p is the pressure, Y_{ox} is the oxidizer mass fraction and $A = A(x)$ is the cross-section area of the geometry. The effects of fuel addition are accounted through steady source term $\mathbf{H}_f$, where $\dot{\omega}_f = C_{f/O}\dot{\omega}_{ox}$ with constant $C_{f/O}$ representing fuel-to-oxidizer ratio and a sinusoidal spatial distribution is used to model the oxidizer reaction, $\dot{\omega}_{ox}=k_f\bar{\rho}\bar{Y}_{ox}\left(1+\sin\left(-\dfrac{\pi}{2}+\dfrac{x-l_s}{l_f-l_s}2\pi\right)\right)$, $(\forall\ l_s<x<l_f)$, where l_s and l_f are the axial locations of the beginning and end of the combustion zone. The reaction constant k_f is selected to ensure that the oxidizer is consumed within the specified combustion zone. The unsteady combustion response is accounted in the source term, $\mathbf{H}_q$, using the n-τ model [17], $\dot{q}'''=\bar{\dot{q}}\cdot n\cdot\alpha(x)\dfrac{p(x,t-\tau)-\bar{p}(x)}{\bar{p}(x)}$, which relates the unsteady heat release to the pressure oscillations through an index, n and a time lag constant, τ. Here $\bar{\dot{q}}$ is the integral mean combustion heat release and $\alpha(x)$ is a scaling function following a normal distribution, $\alpha(x)=\dfrac{1}{\sigma\sqrt{2\pi}}\exp\left(-\dfrac{(x-\mu)^2}{2\sigma^2}\right)$. This model was previously used [18] to simulate combustion instability in a longitudinal rocket combustor,

For simplicity, the linearized version of Eq. (2) is used for the studies in ROM development,

$$\bar{\Gamma}_p\frac{\partial\mathbf{Q}'_p}{\partial t}+\frac{\partial\bar{A}_p\mathbf{Q}'_p}{\partial x}=\bar{D}_p\mathbf{Q}'_p \tag{3}$$

where $\mathbf{Q}'_p=\begin{pmatrix}p' & u' & T' & Y'_{ox}\end{pmatrix}^{\mathrm{T}}$, $\bar{\Gamma}_p=\left.\dfrac{\partial\mathbf{Q}}{\partial\mathbf{Q}_p}\right|_{\bar{\mathbf{Q}}_p}$, $\bar{A}_p=\left.\dfrac{\partial\mathbf{E}}{\partial\mathbf{Q}_p}\right|_{\bar{\mathbf{Q}}_p}$ and $\bar{D}_p=\left.\left(\dfrac{\partial\mathbf{H}}{\partial\mathbf{Q}_p}+\dfrac{\partial\mathbf{H}_q}{\partial\mathbf{Q}_p}\right)\right|_{\bar{\mathbf{Q}}_p}$.

Fluctuating conditions inside the computational domain are obtained by specifying a periodic upstream mass flow rate, $\dot{m}'(t)$, oscillating around the mean value at the inlet, $\dot{m}_0$,

$$\dot{m}'(t)=\dot{m}_0\frac{\varepsilon}{N_f}\sum_{k=1}^{N_f}\sin\left(2\pi\left(f_0+\Delta f\right)t\right) \tag{4}$$

where f_0 is the initial frequency; Δf represents the fundamental frequency increment and N_f is the total number of frequencies included in the forcing function. The fundamental period T_p is determined by Δf such that $T_p = 1/\Delta f$.

Note that if $\Delta f = f_0$, Eq. (4) represents a standard Fourier series although herein we generally take $\Delta f < f_0$ so that Eq. (4) differs slightly from a Fourier series.

B. Construction of POD eigen-bases for vector equations

POD eigen-bases are calculated based on the CFD solutions, $\mathbf{Q}'_p(x,t)$ obtained from Eq. (3),

$$P(x)\mathbf{Q}'_p(x,t) \approx \sum_{n=1}^{N_p} \hat{a}_n(t)\sigma_n \mathbf{\Phi}_n(x) = \sum_{n=1}^{N_p} \hat{a}_n(t)\sigma_n \begin{pmatrix} \phi_{p,n}(x) \\ \phi_{u,n}(x) \\ \phi_{T,n}(x) \\ \phi_{Y_{ox},n}(x) \end{pmatrix} = \sum_{n=1}^{N_p} a_n(t) \begin{pmatrix} \phi_{p,n}(x) \\ \phi_{u,n}(x) \\ \phi_{T,n}(x) \\ \phi_{Y_{ox},n}(x) \end{pmatrix} \tag{5}$$

where σ_n is the singular value of the n^{th} POD mode (scalar), $a_n(t)$ is the n^{th} POD temporal mode (scalar), and the n^{th} eigen-mode, $\mathbf{\Phi}_n(x)$, is an orthonormal vector function,

$$\int_X \mathbf{\Phi}_n^{\mathrm{T}}(x)\mathbf{\Phi}_n(x)dx = \begin{cases} 1, \text{ if } k = n \\ 0, \text{ otherwise} \end{cases}, \quad X = \{0 \le x \le L\} \tag{6}.$$

It should be noted that, unlike in the scalar equation case, to obtain reasonably scaled POD eigen-bases for the vector variables, a normalization matrix $P(x)$ must be used before calculating the POD eigen-bases. Likewise, to reconstruct the CFD solutions using the POD eigen-bases, the matrix $P(x)$ again needs to be included,

$$\mathbf{Q}'_p(x,t) \approx P^{-1}(x)\sum_{n=1}^{N_p} a_n(t) \begin{pmatrix} \phi_{p,n}(x) \\ \phi_{u,n}(x) \\ \phi_{T,n}(x) \\ \phi_{Y_{ox},n}(x) \end{pmatrix} \tag{7}.$$

Definitions of the normalization matrix, P(x), are considered later.

C. Model reduction of Euler equations

The application of the POD-Galerkin method to the linearized Euler equations (Eq. (3)) is briefly introduced here. Additional details can be found in Ref [11]. Upon obtaining the eigen-bases as in Eq. (5), the target governing equation is projected onto the k^{th} eigen-mode $\mathbf{\Phi}_k(x)$ throughout the whole computational domain. Before the projection, the governing equation needs to be normalized by pre-multiplying by the matrix $P(x)$,

$$\int_X \mathbf{\Phi}_k^{\mathrm{T}}(x)P(x)\left(\frac{\partial \mathbf{Q}'_p(x,t)}{\partial t} + \bar{\Gamma}_p^{-1}(x)\frac{\partial \bar{A}_p(x)\mathbf{Q}'_p(x,t)}{\partial x}\right)dx = \int_X \mathbf{\Phi}_k^{\mathrm{T}}(x)P(x)\bar{\Gamma}_p^{-1}(x)\bar{D}_p(x)\mathbf{Q}'_p(x,t)dx \tag{8},$$

Substituting the POD expansion, Eq. (7) into Eq. (8) and using a numerical quadrature to approximate the integrals,

$$\sum_{n=1}^{N_p}\left\{\sum_{i=1}^{\mathrm{NI}}\boldsymbol{\Phi}_{k,i}^{\mathrm{T}}P_i P_i^{-1}\boldsymbol{\Phi}_{n,i}\Delta x_i\right\}\dot{a}_n(t) + \sum_{n=1}^{N_p}\left\{\sum_{i=1}^{\mathrm{NI}}\left(\boldsymbol{\Phi}_{k,i}^{\mathrm{T}}P_i\bar{\Gamma}_{p,i}^{-1}\left(\frac{\delta\bar{A}_p P^{-1}\boldsymbol{\Phi}_n}{\delta x}\right)_i - \boldsymbol{\Phi}_{k,i}^{\mathrm{T}}P_i\bar{\Gamma}_{p,i}^{-1}\bar{D}_{p,i}P_i^{-1}\boldsymbol{\Phi}_{n,i}\right)\Delta x_i\right\}a_n(t) = 0 \tag{9}.$$

Following the model reduction procedure in Ref [11] and using a consistent discretization scheme to approximate the gradient term in Eq. (9) as discussed in Section II, an ODE system can be obtained with the contributions from boundary conditions appearing as a source term on the right-hand-side,

$$\begin{cases} M\dfrac{d\mathbf{a}(t)}{dt} - L\mathbf{a}(t) = \mathbf{h}(t) \\ a_k(0) = \displaystyle\sum_{i=1}^{\mathrm{NI}}\boldsymbol{\Phi}_{k,i}^{\mathrm{T}}\mathbf{Q}'_p(x_i, t=0)\Delta x_i \quad (\text{initial conditions}) \end{cases} \tag{10}$$

where $\mathbf{a}(t) = \left[a_1(t) \quad \cdots \quad a_k(t) \quad \cdots \quad a_{N_p}(t)\right]^{\mathrm{T}}$,

$\mathbf{h}(t) = \left[h_1(t) \quad \cdots \quad h_k(t) \quad \cdots \quad h_{N_p}(t)\right]^{\mathrm{T}}$ with contributions from boundary conditions, $h_k(t) = F_k\left(\dot{m}'(t)\right)$,

L is the stiffness matrix which describes the dynamics of the reduced ODE system.

IV. Overview of Test Problem

A constant-area duct is set up for the ROM development as shown in Fig. 1 with an acoustically open boundary condition at the outlet and a mass flow perturbation specified at the inlet. For a typical computation, the steady state numerical solution of Eq. (2) is computed first with a constant mass flow rate, $\dot{m}_0$ at the inlet. Representative steady state solutions are shown in Fig. 2(a), the temperature of which has the general character of an Arrhenius term with a rapid increase followed by an asymptotic approach to the final temperature. The upstream boundary condition is then switched to a temporally varying periodic condition as defined in Eq. (4) and the time-accurate computation is continued until stationary conditions are reached.

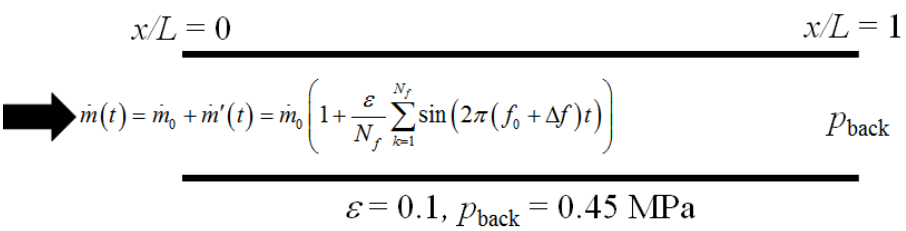

Figure 1 Computational setup for the one-dimensional Euler equations.

The solutions are tabulated and stored periodically (i.e., at several time-levels within a forcing period) thereby generating a rectangular matrix that can be used as a database for fitting eigen-bases by means of the POD procedure detailed below. The POD eigen-bases are then applied to the governing linear or nonlinear PDE to derive the reduced-order ODE formulation (or ROM).

Before delving into the POD eigen-bases generation and reduced-order model development, it is important to get a basic understanding of the inherent system response of the test problem. For this purpose, no unsteady combustion response is included in the test problem (i.e. n is set to 0 in Eq. (3)). To identify the system response, several sets of CFD solutions are calculated using different mass flow forcing frequencies at the inlet following the FTF/FDF (Flame Transfer/Describing Function) approach [19]. The perturbation level ε in Eq. (4) is set to 0.1. For each case, only one frequency is included in the forcing function and the amplitudes and phase relations with regard to the boundary perturbations are then calculated at different locations accordingly. The resulting amplitudes and phases of pressure (p') and velocity (u') fluctuations are plotted versus the forcing frequencies and shown in Fig. 2(b). A strong resonant system response at approximately 1350Hz can be clearly seen, which corresponds to the 1st fundamental acoustic frequency (1L) determined by the duct length and mean speed of sound. We point out that this natural system response is a unique characteristic of the Euler equations and does not appear in the scalar equation case. This is due to the simultaneous presence of both forward and backward moving waves in the Euler system, which naturally gives rise to resonant (standing) wave solutions that correspond to the fundamental acoustic modes.

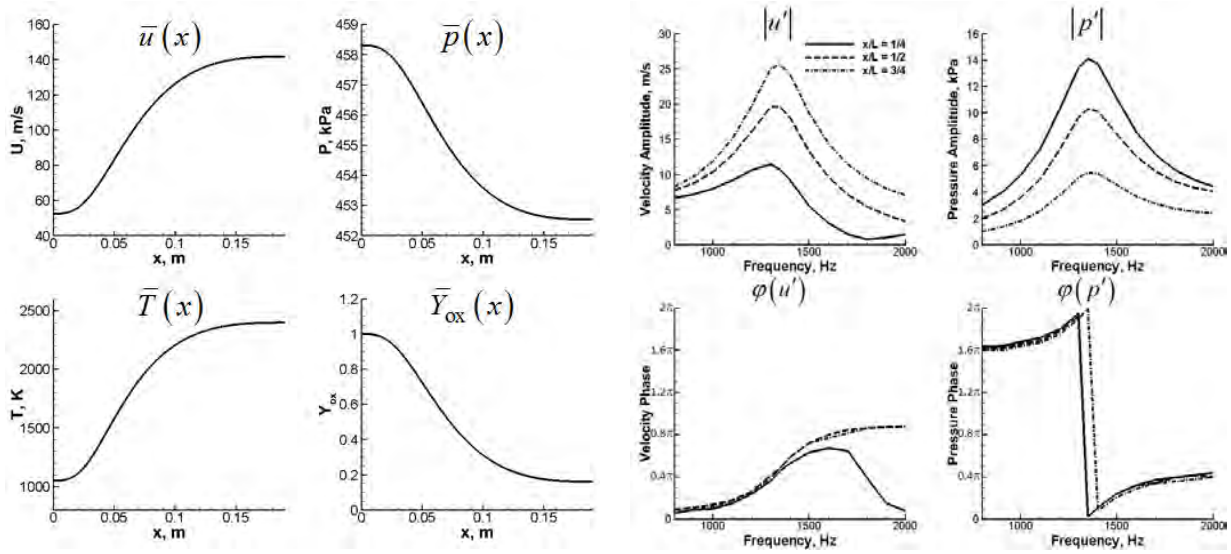

(a) Steady state solutions to Eq. (2)

(b) Generic system responses (top: limit cycle amplitude; bottom: phase angle)

Figure 2 Characteristics of the (a) Steady state solutions to Eq. (2) and (b) Identified generic system responses of the test problem.

V. Results

A. POD Verification

The effectiveness of POD eigen-bases for representing the original numerical solutions is verified in the same way as in the scalar equation. At the same time, we also validate the two bases per frequency rule identified in the scalar equation studies (see conclusion 1 in Section II). The cases used for POD verification are summarized in Table 1. Three cases are selected with different forcing functions from single to multiple frequencies and POD eigen-bases are generated for each case. As discussed earlier in regard to Eq. (5), the CFD solutions to the Euler equations need pre-treatment before the POD eigen-basis calculation. In this section, the four variables (u', p', T' and Y'_{ox}) are normalized by the maximum values of the respective fluctuating quantity throughout the whole domain (i.e. $P(x) = \mathrm{diag}\left(1/p'_{\max}, 1/u'_{\max}, 1/T'_{\max}, 1/Y'_{ox,\max}\right)$ where $p'_{\max} = \mathrm{Max}\left\{p'(x,t)\right\}$, $\forall\ 0 \le x \le L$ and t etc.). It can be readily seen that the two bases per frequency rule is still valid for the linearized Euler equations.

Case No.	f_0, Hz	Δf, Hz	# of forcing frequencies	Rank of POD matrix
G1	1000	--	1	2
G2	1000	250	3	6
G3	750	250	5	10

Table 1 Summary of cases used in studies of POD verifications.

Similar to the scalar equation studies, the test solutions are reconstructed using the POD eigen-bases as given in Eq. (7) and then compared with the numerical solutions using the L_2-norm defined,

$$L_2\text{-norm}\left(N_p\right) \text{ of variable } q_k \text{ at } x_i = \frac{\int\left\{q'_k(x_i,t) - \mathbf{p}_k^{\mathrm{T}}(x_i)\sum_{n=1}^{N_p} a_n(t)\boldsymbol{\Phi}_n(x_i)\right\}^2 dt}{\int q'^2_k(x_i,t)\,dt} \qquad (11),$$

where $\mathbf{p}_k^{\mathrm{T}}(x_i)$ is the k^{th} row of matrix $P^{-1}(x_i)$. The L_2-norms are plotted for each case in Fig. 3 against the number of POD modes included in the solution reconstruction of all four variables (u', p', T' and Y'_{ox}). For all three cases, the L_2-norms saturate and reach good accuracy after including a mode number equal to the matrix rank thereby validating the effectiveness of the POD eigen-bases for capturing the original dynamics. The verified POD modes here will be carried on next to build the ROMs in following section. So far, both scalar and Euler equation(s) studies show consistency in the POD eigen-bases generation.

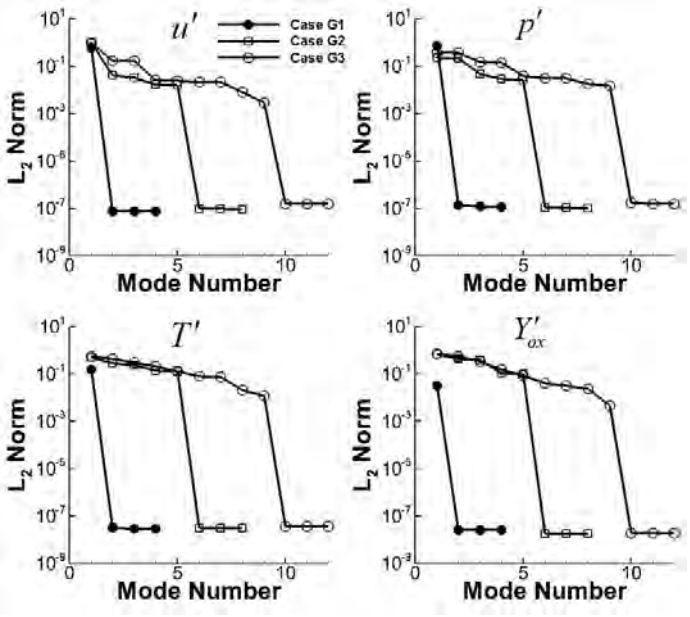

Figure 3 POD verifications of cases in Table 1 (L_2-norm calculated at $x/L = 0.5$).

B. ROM Characteristics for Vector Equations

Knowing the number of POD modes needed for ROM development in previous section, the characteristics of the ROM are studied in this section for the three cases in Table 1. The eigen-value spectra of the ROM stiffness matrices (L in Eq. (10)) are investigated and shown in Fig. 4. In all cases, the number of POD modes included in the ROM development is equal to the rank of POD matrix. For Cases G1 and G3, all eigen-values have negative real parts (σ) which, as discussed in the scalar equation studies, indicates that the corresponding ROM's will be stable. Solving the ROM equation for these two cases using the same forcing as used in the CFD solution gives reconstructed solutions that are indeed in excellent agreement with the CFD results as shown in Fig. 5. The ROM's are able to reproduce the original CFD solutions and show no unphysical or unstable behavior.

Though ROM development for Case G1 and G3 follows the knowledge learned from the scalar equation studies, Case G2 shows some differences. An unstable mode is detected in Case G2 (highlighted by the red circle in Fig. 4) even though all necessary POD modes are included to build the ROM. This unstable mode leads to unphysical growth in the ROM solution as shown in Fig. 6. The growth rate of the unstable eigenvalue is small, enabling the ROM solution to compare well with the CFD solution at early times (0.025 to 0.07s shown in the zoomed-in box in the *p'* plot) but the ROM prediction goes off track at longer times as the unstable mode starts to dominate. It should be noted that the POD modes used for the ROM development are calculated using CFD solutions corresponding to one cycle (defined based on Δf in Table 1), the same as in the scalar case; here, CFD solutions from 0.025 to 0.029s are selected and so the ROM solution is technically valid based on the information given. However, the appearance of the unstable mode strongly impacts the ROM's predictive capability.

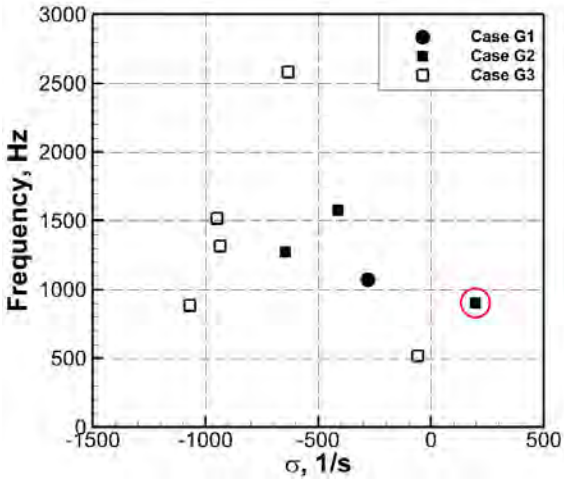

Figure 4 Eigen-value spectrum of ROM stiffness matrix for Cases G1 to G3 in Table 1.

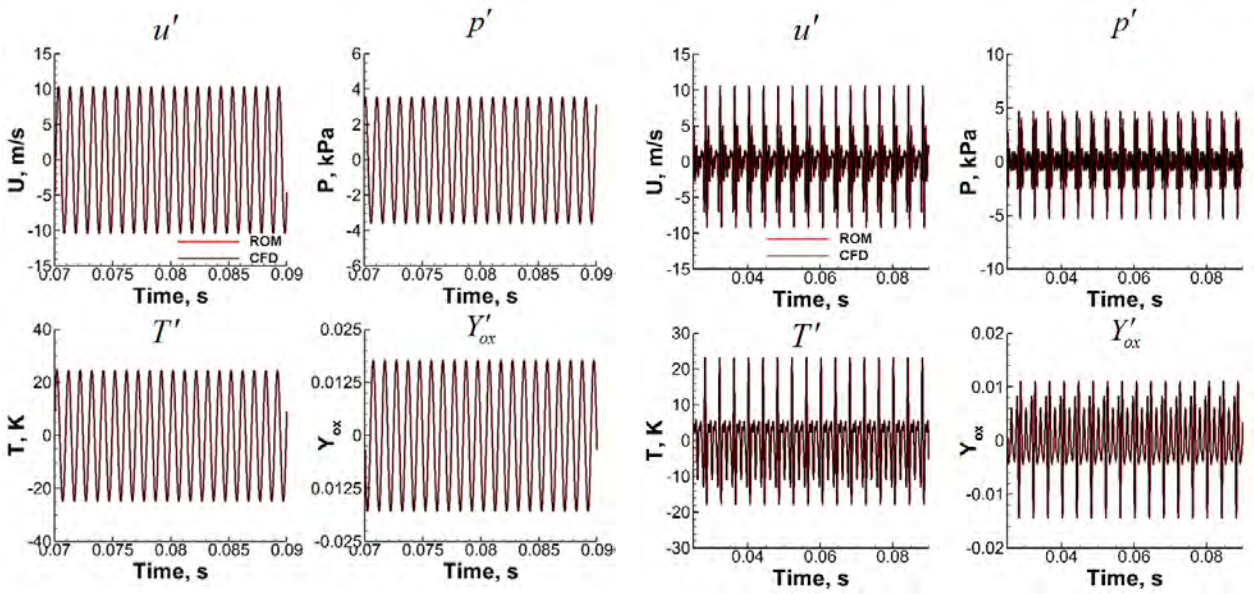

(a) Case G1 (b) Case G3

Figure 5 ROM and CFD solutions comparison at *x*/*L* = 0.5 for Cases G1 to G3 in Table 1.

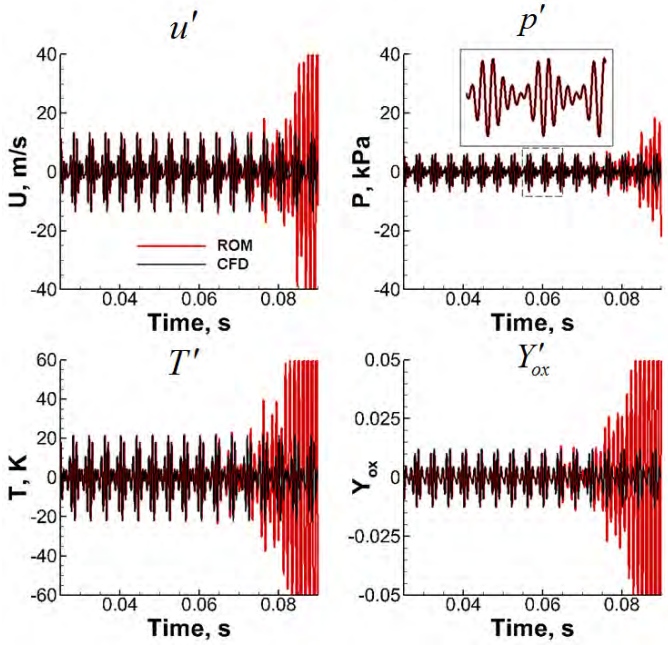

Figure 6 ROM and CFD solutions comparison at x/L = 0.5 for Cases G2 in Table 1.

C. Effects of normalization methods on ROM characteristics

To investigate the causes of the unstable mode seen in Fig. 4, three different normalization methods are tried for Case G2 to assess their effects on the numerical stability of the ROM. The methods used for these studies are summarized in Table 2. Method III is the one that was used previously for the results shown in Figs. 4 - 6 above.

Variables	I	II	III
u'	×	▶	Δ
p'	×	▶	Δ
T'	×	▶	Δ
Y'_{ox}	×	×	Δ

×: no normalization; ▶: domain averaged mean value, e.g. $p_{\text{ref}} = \frac{1}{L}\int_0^L \overline{p}(x)\,dx$

Δ: Maximum value of all points, e.g. $p_{\text{ref}} = \text{Max}\left\{p'(x,t)\right\},\ \forall\ 0 \le x \le L$ and t

Table 2 Summary of normalization methods used in studies of ROM stability issues for Case G2.

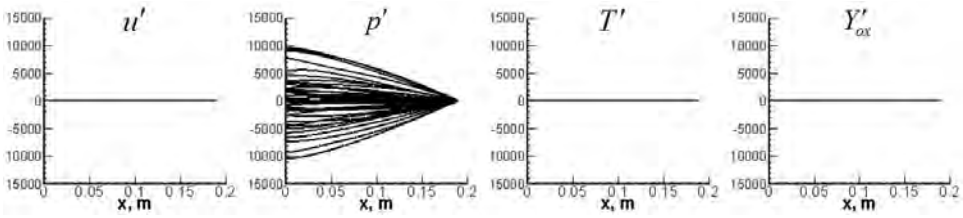

(a) Method I

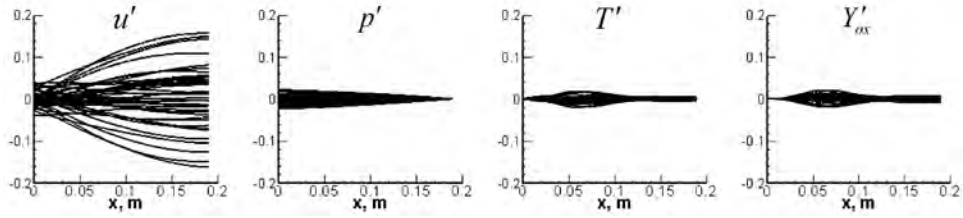

(b) Method II

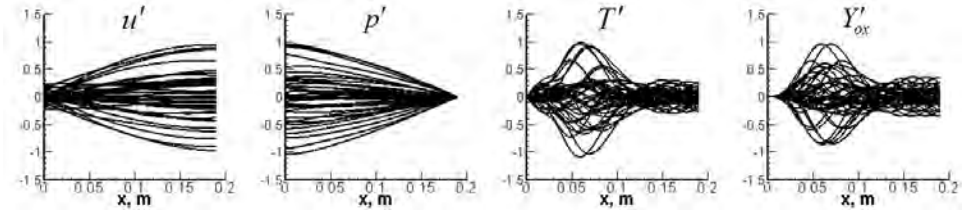

(c) Method III

Figure 7 Comparisons of normalized CFD solutions using methods in Table 2.

Before proceeding to investigations of normalization effects on the ROM characteristics, the normalized solutions used for POD eigen-bases generation are compared for the different methods in Fig. 7. As expected, with no normalization (Method I), the dominance of *p'* overwhelms the other three variables (*u'*, *T'* and Y'_{ox}). By using mean values (Method II), amplitudes of *p'*, *T'* and Y'_{ox} are comparable while *u'* contributes more than the other three variables in POD eigen-bases generation by a factor of approximately 10 so the mode shapes of resulting POD eigen-functions are expected to be governed by the velocity fluctuations. Method III seems to be optimum in keeping four variables within similar fluctuating levels, which makes the contributions from each variable to the POD eigen-bases generation comparable.

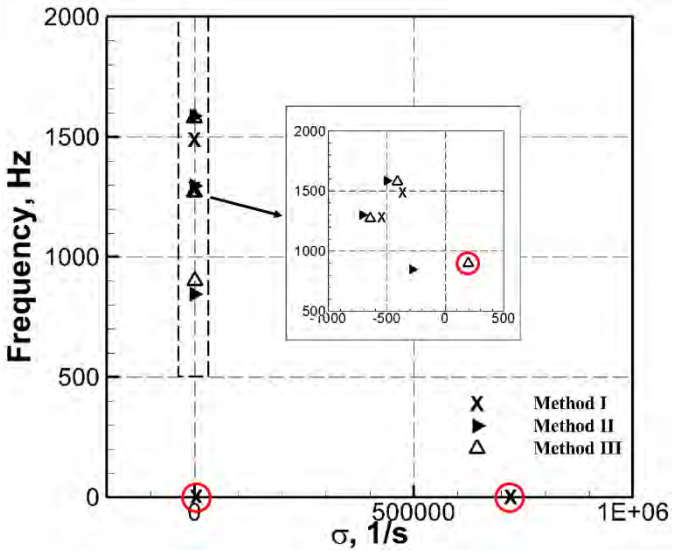

Figure 8 Comparisons of ROM eigen-values using different normalization methods in Table 2.

An overview of the developed ROMs' eigen-values for the different normalization methods is given in Fig. 8 with unstable modes highlighted by red circles. First, it can be seen that the ROM can be stabilized by using Method II, which enables the ROM to reproduce the original CFD solutions as shown in Fig. 9 and no unphysical or unstable behavior seen in Fig. 6 is present. Second, with no normalization, the resulting ROM shows a very large σ value, which can lead to unreasonable growth and totally derail the ROM predictions.

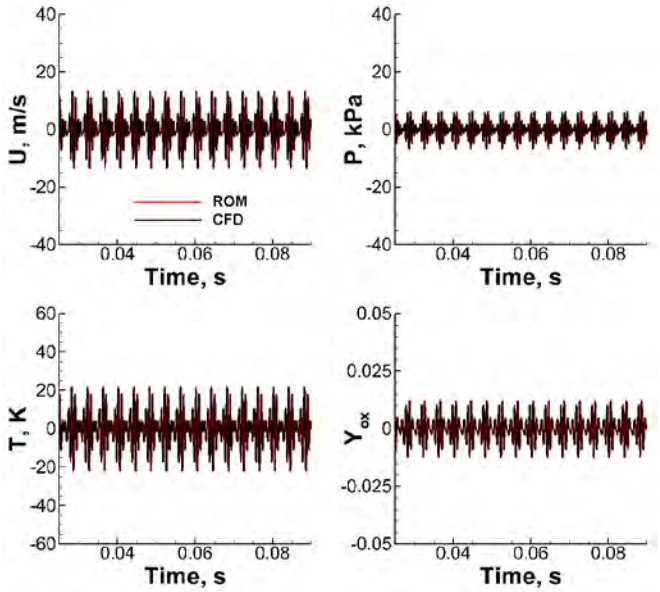

Figure 9 ROM and CFD solutions comparison at x/L = 0.5 for Cases G2 using Method II in Table 2.

Having determined that the unstable mode identified in Fig. 4 can be avoided by using a different normalization method for Case G2, we next test the validity of Method II for the other two cases in Table 1. The corresponding ROM eigen-value spectrum is shown in Fig. 10. It can be seen that the ROM for Case G1 is still stable using Method II for normalization. However, an unstable mode (red circled) can be observed in the ROM for Case G3 at the highest frequency (~3200Hz) with a large σ value (>600s^{-1}). Based on the observation here, it seems that a valid normalization method for one case does not necessarily guarantee a universal numerical stability for the other cases. Moreover, the effects of normalization methods seem to be case-dependent and, in fact, are reliant on the forcing function, which determines the spatial mode shapes of CFD solution. In is noteworthy that Method II fails for Case G3, which only involves two additional frequencies (750 and 1750Hz) compared to the stable Case G2.

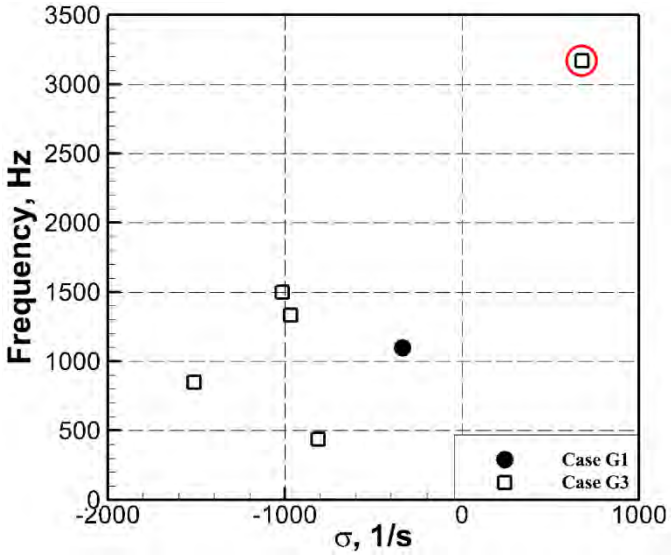

Figure 10 ROM eigen-value spectrum for Cases G1 and G3 using Method II.

D. Effects of Normalization Methods on ROM Predictive Capability

After obtaining some basic understanding of how normalization methods can affect ROM stability, the predictive capabilities of ROMs' developed using different normalization methods are assessed in this section. Studies are performed for ROMs developed using both single- and multi-frequency forcing.

Single-frequency forcing

Two single-frequency forcing functions are used to train ROMs for predictive capability investigations here, one of which is at 1000Hz (Case G1 in Table 1) and the other one is chosen to be 1350Hz (denoted as Case G4 here),

which corresponds to the natural system frequency identified in Fig. 2(b). The studies here are focused on how variable normalization affects the resulting ROM's predictive capability.

For both Case G1 and G4, Method II and III are chosen for ROM predictive capability evaluations. The ROM predictive capability is evaluated in a different way compared to the previous scalar equation studies. Here, the ROMs are used to predict the limit cycle amplitude and phase angle at different input frequencies, which are then compared with CFD results as shown in Fig. 10. Consistent with observations in the scalar equation studies, the two ROMs are able to predict the correct amplitude and phase angle at the forcing frequencies for both cases. The Case G1 ROMs are only able to capture responses at 1000Hz while predictions at other frequencies are poor, which is expected from scalar equation studies (Conclusion 5 in section II). Applying different normalization methods for Case G1 does not change the overall ROM performance.

The Case G4 ROMs show more capabilities for predicting frequency response not included in the forcing function. The Method II ROM is able to capture the overall trend of the system response, but seems to predict a faster amplitude decay versus frequency than the CFD solution does. Interestingly, switching the normalization method seems to have more significant effects than in Case G1. The Method III ROM shows a sharper resonant peak than Method II in limit cycle amplitude, which can also be reflected by an even faster amplitude decay at frequencies not equal to 1350Hz. This might be attributed to the fact that Method III puts more comparable weightings on each variable in generating POD eigen-bases while, in Method II, the eigen-bases for ROM development are dominated by velocity fluctuations (u'), but further investigations are needed.

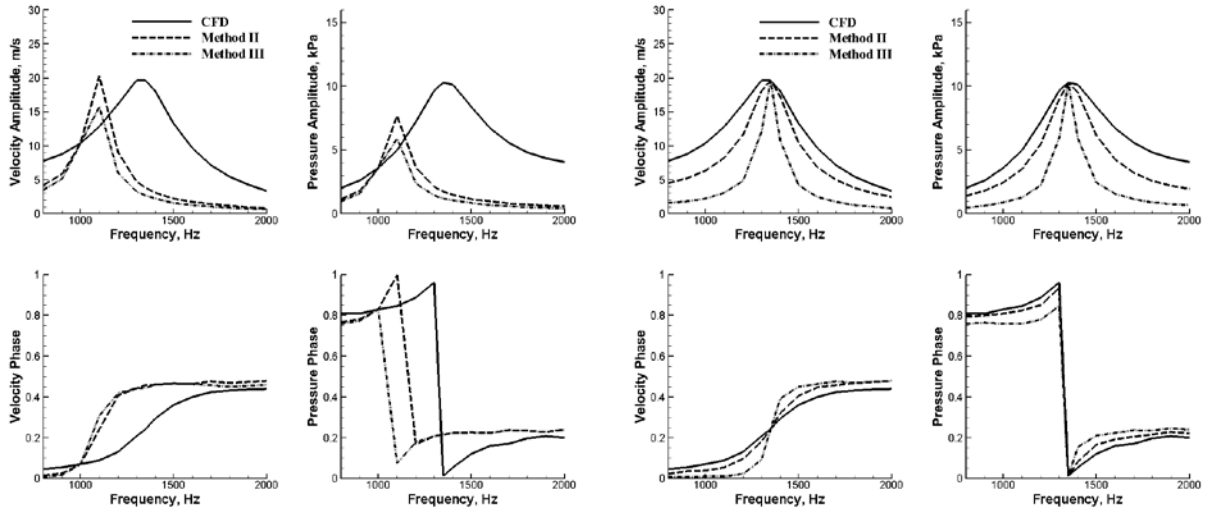

(a) Case G1 ROM (1000Hz forcing) (b) Case G4 ROM (1350Hz forcing)

Figure 11 Comparisons of ROM predictive capability using different normalization methods at x/L = 0.5 for Case G1 and G4.

Multi-frequency forcing

The next set of evaluations is carried out for ROMs trained using multi-frequency boundary forcing (Case G2 & G3 in Table 1). Method II and III are used for comparisons to assess the effects of normalization strategies for the vector system, which are shown in Fig. 11. It has already been shown in Fig. 8 that Method II generates stable ROM while Method III can cause numerical instability issues for Case G2, which leads to a total failure in the ROM predictions of limit cycle amplitude and phase angle, while the stable ROM (from Method II) is able to capture the overall CFD solution trend as shown in Fig. 12(a).

For Case G3, on the other hand, we have noted that Method II is unstable and Method III is stable and the results here confirm that Method III is able to obtain very good agreement with the CFD solutions. Further, by comparing the valid ROM from each case (Method II for Case G2 and Method III for Case G3), it can be seen that by adding two more frequencies (750 and 1750Hz) in the forcing function, the resulting ROM predictive capability can be improved a lot, which is consistent with Conclusion 5 from scalar equation studies, and confirms the value of applying forcing functions with richer frequency content in the ROM development.

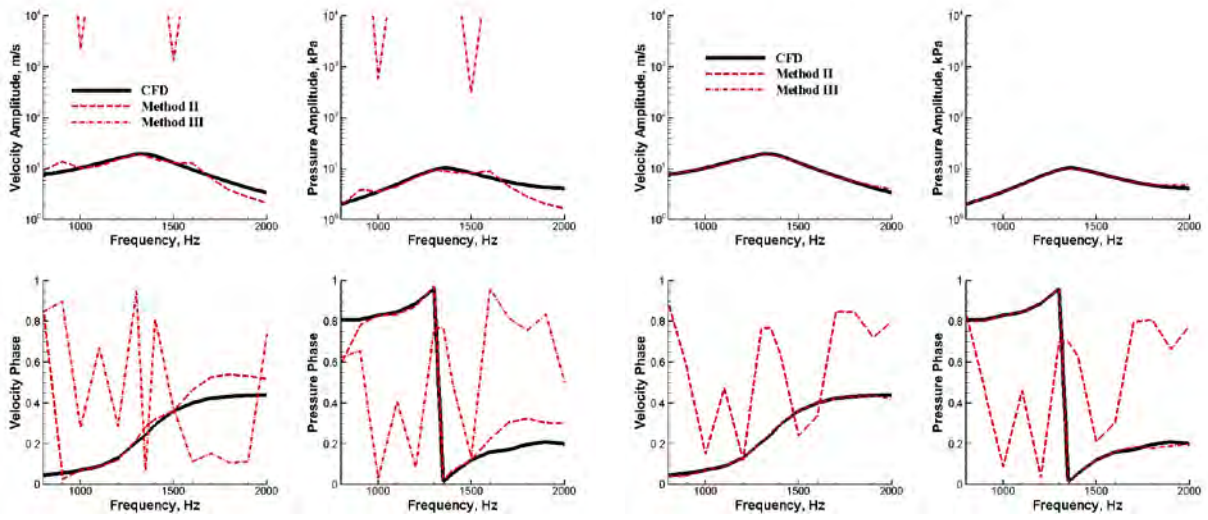

(a) Case G2 (b) Case G3

Figure 12 Comparisons of ROM predictive capability using different normalization methods for Case G2 & G3 in Table 1 at $x/L = 0.5$.

VI. Conclusions

Explorations of the POD/Galerkin method for developing a reduced order model (ROM) for the linearized reactive Euler equations are performed as an extension of previous studies using a reaction-advection scalar equation. Consistent with the previous scalar equation study, the approach utilizes CFD solutions to obtain the POD basis vectors, which are then used within a Galerkin formulation to reduce the governing partial differential equations to a set of ordinary differential equations (ODE). The studies in this paper are focused on two objectives: first, to validate the conclusions from the scalar equation study for the Euler equations; second, to identify specific issues present in ROM development for vector equations as a background for future investigations using the full Navier-Stoke equations.

In Euler equations studies, consistent conclusions can be reached as in the scalar equation case with regard to the number of POD modes required for ROM construction and the enhancement of the predictive capability enhancement by enriching the frequency content of the forcing function used to train the ROM. In other words, we are able to confirm that the two bases per frequency rule remains operative for the Euler equations and the addition of multiple frequencies improves the ROM prediction for a broader frequency band.

The major issue identified in the ROM development of vector equations is the need to normalize the vector variables used to generate the coupled POD eigen-bases, which is not needed in the scalar equation. Without normalization, we observe strong unstable behavior of the ROM eigenvalue spectrum, rendering the corresponding ROM incapable of predicting the correct system response. Normalizing the variables by the maximum value in the domain provides stable behavior for some cases, but unstable modes are observed for other cases. Alternate normalizations such as using the mean value of the variables stabilizes some of the previously unstable cases, but destabilizes other stable cases. The unstable modes are shown to lead to numerical stability problems, which are characterized by unphysical amplitude growth in the ROM predictions, while the correct CFD solution reaches a limit cycle (i.e., no growth).

Overall, applying ROM capabilities to the prediction of combustion instability remains an important, but highly challenging task. Such models have the potential to provide effective predictions at a fraction of the cost needed for solving the original partial differential equation set. However, as the present paper points out, significant issues remain in formulating the ROM for vector systems such as the Euler equations. More studies need to be done to understand the effects of variable normalization on the ROM construction and the proper normalization procedure to avoid spurious unstable modes. A possible solution is to re-define the inner product needed for the coupled POD eigen-bases calculation so that the coupling between different unsteady quantities can be incorporated naturally in POD modes generation. An example of that can be found in Ref. [16], which will be a starting point for our future studies.

Reference

1. Bergmann, M., Bruneau, C. H., and Iollo, A. "Enablers for robust POD models," *Journal of Computational Physics* Vol. 228, No. 2, 2009, pp. 516-538.

2. Rowley, C. W. "Model Reduction for Fluids using Balanced Proper Orthogonal Decomposition," *International Journal of Bifurcation and Chaos*, 2005.

3. Rowley, C. W., Colonius, T., and Murray, R. M. "Model reduction for compressible flows using POD and Galerkin projection," *Physica D: Nonlinear Phenomena* Vol. 189, No. 1-2, 2004, pp. 115-129.

4. Barbagallo, A., Dergham, G., Sipp, D., Schmid, P. J., and Robinet, J.-C. "Closed-loop control of unsteadiness over a rounded backward-facing step," *Journal of Fluid Mechanics* Vol. 703, 2012, pp. 326-362.

5. Barbagallo, A., Sipp, D., and Schmid, P. J. "Closed-loop control of an open cavity flow using reduced-order models," *Journal of Fluid Mechanics* Vol. 641, 2009, p. 1.

6. Barbagallo, A., Sipp, D., and Schmid, P. J. "Input–output measures for model reduction and closed-loop control: application to global modes," *Journal of Fluid Mechanics* Vol. 685, 2011, pp. 23-53.

7. Lieu, T., and Farhat, C. "Adaptation of Aeroelastic Reduced-Order Models and Application to an F-16 Configuration," *AIAA Journal* Vol. 45, No. 6, 2007, pp. 1244-1257.

8. Lucia, D. J., Beran, P. S., and Silva, W. A. "Reduced-order modeling: new approaches for computational physics," *Progress in Aerospace Sciences* Vol. 40, No. 1-2, 2004, pp. 51-117.

9. Munipalli, R., Zhu, X., Menon, S., and Hesthaven, J. "Model Reduction Opportunities in Detailed Simulations of Combustion Dynamics," *52nd Aerospace Sciences Meeting*. National Harbor, Maryland, 2014.

10. Huang, X., and Baumann, W. T. "Reduced-Order Modeling of Dynamic Heat Release for Thermoacoustic Instability Prediction," *Combustion Science and Technology* Vol. 179, No. 3, 2007, pp. 617-636.

11. Huang, C., Anderson, W. E., Merkle, C., and Sankaran, V. "Exploration of POD-Galerkin Method in Developing a Flame Model for Combustion Instability Problems," *7th AIAA Theoretical Fluid Mechanics Conference*. Atlanta, GA, 2014.

12. Rempfer, D. "On Low-Dimensional Galerkin Models for Fluid Flow," *Theoretical and Computational Fluid Dynamics* Vol. 14, 2000, pp. 75–88.

13. Noack, B. R., Papas, P., and Monkewitz, P. A. "The need for a pressure-term representation in empirical Galerkin models of incompressible shear flows," *Journal of Fluid Mechanics* Vol. 523, 2005, pp. 339-365.

14. Willcox, K., and Peraire, J. "BalancedModel Reduction via the Proper Orthogonal Decomposition," *AIAA Journal* Vol. 40, 2002.

15. Barone, M., Segalman, D., Thornquist, H., and Kalashnikova, I. "Galerkin Reduced Order Models for Compressible Flow with Structural Interaction," *46th AIAA Aerospace Sciences Meeting and Exhibit*. Reno, Nevada, 2008.

16. Barone, M. F., Kalashnikova, I., Brake, M. R., and Segalman, D. J. "Reduced Order Modeling of Fluid/Structure Interaction." Sandia National Laboratories, 2009.

17. Crocco, L., Grey, J., and Harrjet, D. T. "On the Importance of Sensitivity Time Lag in Longitudinal High-frequency Rocket Combustion Instability," *Jet Propulsion* Vol. 28, No. 12, 1958, pp. 841-843.

18. Smith, R. J., Xia, G., Sankaran, V., Anderson, W. E., and Merkle, C. L. "Computational Investigation of Acoustics and Instabilities in a Longitudinal Mode Rocket Combustor," *AIAA Journal* Vol. 46, 2008.

19. Noiray, N., Durox, D., Schuller, T., and Candel, S. "A unified framework for nonlinear combustion instability analysis based on the flame describing function," *Journal of Fluid Mechanics* Vol. 615, 2008, p. 139.